Int J Thermophys (2007) 28:1718–1729
DOI 10.1007/s10765-007-0214-y

Thermal Conductivity of Xonotlite Insulation Material

Gaosheng Wei · Xinxin Zhang · Fan Yu

Published online: 15 August 2007

Abstract A surface-contact hollow cubic model is developed for coupled heat transfer of gas and solid in xonotlite-type calcium silicate insulation material based on its microstructure features. Through one-dimensional heat conduction analysis in the unit cell structure, a conductive thermal conductivity expression is obtained. A transient hot strip method is used to measure the thermal conductivity of xonotlite from 300 to 970 K and from 0.045 Pa to atmospheric pressure. The spectral specific extinction coefficients are derived from transmission measurements on a thin xonotlite sample performed with a Fourier transform infrared (FTIR) spectrometer. The results show that the specific spectral extinction coefficients are larger than $7\,m^2 \cdot kg^{-1}$ over the whole measured spectra, and the diffusion approximation equation is a reasonable description of radiative heat transfer in xonotlite insulation material. The effective thermal conductivity model matches extremely well with the experimental data, which is important for the thermal design and thermal analysis of xonotlite insulation material.

Keywords Extinction coefficient · Insulation · Thermal conductivity · Transient hot strip method · Xonotlite-type calcium silicate

Paper presented at the Seventeenth European Conference on Thermophysical Properties, September 5–8, 2005, Bratislava, Slovak Republic.

G. Wei (✉)
School of Energy and Power Engineering, Key Laboratory of Condition Monitoring and Control for Power Plant Equipment of Ministry of Education, North China Electric Power University, Beijing 102206, P.R. China
e-mail: gaoshengw@126.com

X. Zhang · F. Yu
Department of Thermal Engineering, University of Science and Technology Beijing, Beijing 100083, P.R. China

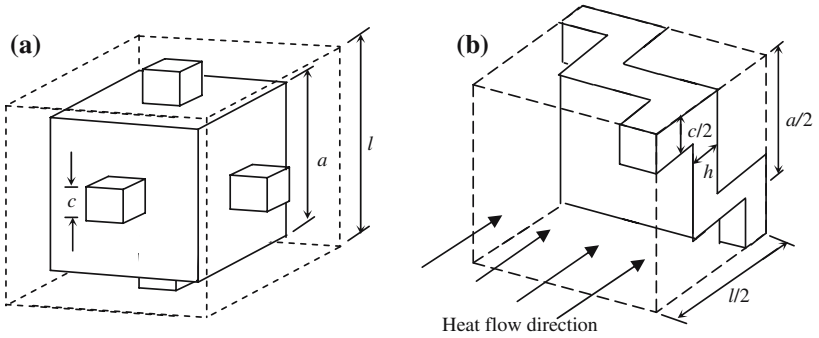

Fig. 1 Surface-contact hollow cubic structure and unit cell model of xonotlite (**a**) surface-contact hollow cubic structure and (**b**) unit cell

1 Introduction

Xonotlite-type calcium silicate ($6CaO \cdot 6SiO_2 \cdot H_2O$) is a synthesized high-porosity insulation material obtained by hydrothermal processing with quartz powder and limestone as the raw material (with $CaO/SiO_2 \approx 1{:}1$). Compared with fire-retardant fiber, xonotlite has excellent insulating performance, such as low thermal conductivity, environmentally friendly, high strength, and a wide temperature range, all of which have been recognized in recent years by researchers and are of broad interest to industry [1–4].

The heat transfer mechanisms in porous insulation materials include solid conduction, gas conduction, and radiation through participating media. Natural convection can always be neglected if the pore in the material is small (<4 mm) [5,6]. The effective thermal conductivity of a porous media depends on its microstructure. In general, the microstructure of porous media is of a random nature. One may use a regular structure to replace the random structure to obtain an effective thermal conductivity. Many microstructure models have been proposed for various porous materials [7–12]. However, those models cannot be used to estimate the effective thermal conductivity of xonotlite-type calcium silicate directly because of its high porosity (>90%) and specific structure features (hollow spherical agglomerates).

In our preceding study [13,14], two unit cell models, the point-contact hollow spherical model and the surface-contact hollow cubic model, are developed to depict the conductive heat transfer in xonotlite-type calcium silicate insulation material, and it is shown that the surface-contact hollow cubic model is a better description of the conductive heat transfer in the material. In this study, based on the surface-contact hollow cubic structure, the analytical expression is derived thoroughly. A diffusion approximation equation is adopted to calculate the radiative thermal conductivity. The model is validated with experimental data. The spectral specific extinction coefficients are obtained by measuring the transmittance spectrum of xonotlite samples of different thicknesses with a Fourier transform infrared (FTIR) spectrometer. The effective thermal conductivities of xonotlite at different temperatures and pressures are measured with a transient hot-strip method.

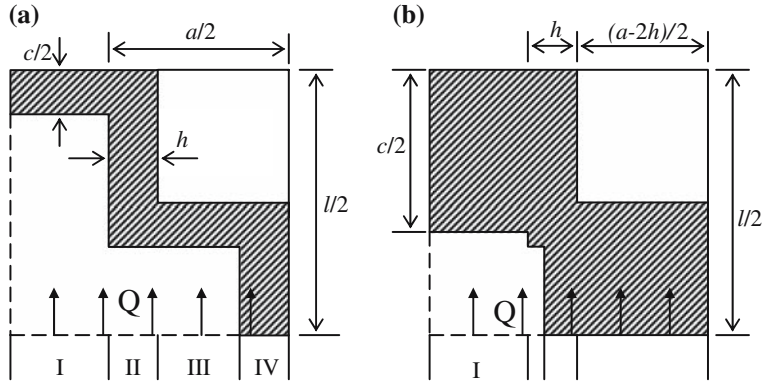

Fig. 2 Unit cell in plane view (**a**) $0 < c < a - 2h$ and (**b**) $a > c > a - 2h$

2 Theoretical Model

2.1 Surface-Contact Hollow Cubic Structure and Conductive Heat Transfer

Through the use of a scanning electronic microscope, it is found that xonotlite is made up of hollow spherical agglomerates interwoven with xonotlite fiber with radii from hundreds to thousands of nanometers [3,4]. By simplification, xonotlite is considered as a periodical array of hollow cubic structures with connecting bars as shown in Fig. 1a. Due to the fact that the shell consists of xonotlite fiber, there exist pores in it; the porosity of the shell is defined as Φ_i. A unit cell of this three-dimensional structure is shown in Fig. 1b. It can be shown that the porosity of the unit cell is [13]

$$\Phi = 1 - (1 - \Phi_i)[(1 - (1 - \gamma_b)^3 - 3\gamma_c^2)\gamma_a^3 + 3\gamma_a^2\gamma_c^2] \tag{1}$$

where $\gamma_a = a/l$, $\gamma_b = 2h/a$, and $\gamma_c = c/a$.

One-dimensional heat conduction is considered in order to derive an analytical expression for the conductive heat transfer. The direction of heat flow is shown in Fig. 1b. The unit cell is divided into four parts as shown in Fig. 2. The conductivity expression is derived by applying the parallel law of thermal resistances. Two cases exist as discussed below.

2.1.1 Case for $0 < c < a - 2h$

Conduction in the unit cell consists of four parts (see Fig. 2a): (I) heat transfer through rectangular $(l-a)/2 \times l/2 \times l/2$, (II) heat transfer through rectangular $h \times l/2 \times l/2$, (III) heat transfer through rectangular $(a-2h-c)/2 \times l/2 \times l/2$, and (IV) heat transfer through rectangular $c/2 \times l/2 \times l/2$. The effective conductivity due to conduction of the unit cell is

$$k_c = (1-\gamma_a)k_{sg1} + \gamma_a\gamma_b k_{sg2} + \gamma_a(1-\gamma_b-\gamma_c)k_{sg3} + \gamma_a\gamma_c k_{sg4} \tag{2}$$

where k_{sg1}, k_{sg2}, k_{sg3}, and k_{sg4} are the effective thermal conductivities corresponding to (I), (II), (III), and (IV), respectively. Each of them, in turn, is also derived separately by applying the parallel law of thermal resistances. The corresponding expressions are as follows:

$$k_{sg1} = \frac{\gamma_a\gamma_c k_g k_{cq}}{(1-\gamma_a\gamma_c)k_{cq} + k_g\gamma_a\gamma_c} + (1-\gamma_a\gamma_c)k_g \tag{3}$$

$$k_{sg2} = \frac{\gamma_a k_g k_{cq}}{(1-\gamma_a)k_{cq} + k_g\gamma_a} + (1-\gamma_a)k_g \tag{4}$$

$$k_{sg3} = \frac{\gamma_a(1-\gamma_b)k_g k_{cq}}{(1-\gamma_a\gamma_b)k_{cq} + k_g\gamma_a\gamma_b} + \frac{\gamma_a\gamma_b k_g k_{cq}}{(1-\gamma_a)k_{cq} + k_g\gamma_a} + (1-\gamma_a)k_g \tag{5}$$

$$k_{sg4} = \frac{\gamma_a(1-\gamma_b-\gamma_c)k_g k_{cq}}{(1-\gamma_a\gamma_b)k_{cq} + k_g\gamma_a\gamma_b} + \frac{\gamma_a\gamma_b k_g k_{cq}}{(1-\gamma_a)k_{cq} + k_g\gamma_a} + \frac{(1-\gamma_a)k_g k_{cq}}{(1-\gamma_a\gamma_c)k_{cq} + k_g\gamma_a\gamma_c} + \frac{\gamma_a\gamma_c k_g k_{cq}}{k_{cq}\gamma_a(1-\gamma_b) + (1-\gamma_a+\gamma_a\gamma_b)k_g} \tag{6}$$

where k_g and k_{cq} are the thermal conductivities of the gas and shell, respectively.

2.1.2 Case for $a > c > a - 2h$

Similarly, conduction in the unit cell also consists of four parts (Fig. 2b): (I) heat transfer through rectangular $(l-a)/2 \times l/2 \times l/2$; (II) heat transfer through rectangular $(a-c)/2 \times l/2 \times l/2$; (III) heat transfer through rectangular $[h-(a-c)/2] \times l/2 \times l/2$; and (IV) heat transfer through rectangular $(a-2h)/2 \times l/2 \times l/2$. The effective conductivity due to conduction of the unit cell is

$$k_c = (1-\gamma_a)k'_{sg1} + \gamma_a(1-\gamma_c)k'_{sg2} + \gamma_a(\gamma_b+\gamma_c-1)k'_{sg3} + \gamma_a(1-\gamma_b)k'_{sg4} \tag{7}$$

where k'_{sg1}, k'_{sg2}, k'_{sg3}, and k'_{sg4} are the effective thermal conductivities corresponding to (I), (II), (III), and (IV), respectively. The corresponding expressions are as follows:

$$k'_{sg1} = \frac{\gamma_a\gamma_c k_g k_{cq}}{(1-\gamma_a\gamma_c)k_{cq} + k_g\gamma_a\gamma_c} + (1-\gamma_a\gamma_c)k_g \tag{8}$$

$$k'_{sg2} = \frac{\gamma_a k_g k_{cq}}{(1-\gamma_a)k_{cq} + k_g\gamma_a} + (1-\gamma_a)k_g \tag{9}$$

$$k'_{sg3} = \gamma_a\gamma_c k_{cq} + \frac{\gamma_a(1-\gamma_c)k_g k_{cq}}{(1-\gamma_a)k_{cq} + k_g\gamma_a} + \frac{(1-\gamma_a)k_g k_{cq}}{(1-\gamma_a\gamma_c)k_{cq} + k_g\gamma_a\gamma_c} \tag{10}$$

$$k'_{sg4} = \frac{\gamma_a(1-\gamma_b)k_g k_{cq}}{k_{cq}\gamma_a(1-\gamma_b) + (1-\gamma_a+\gamma_a\gamma_b)k_g} + \gamma_a(\gamma_b+\gamma_c-1)k_{cq} \times \frac{\gamma_a(1-\gamma_c)k_g k_{cq}}{(1-\gamma_a)k_{cq} + k_g\gamma_a} + \frac{(1-\gamma_a)k_g k_{cq}}{(1-\gamma_a\gamma_c)k_{cq} + k_g\gamma_a\gamma_c} \tag{11}$$

Substituting Eqs. 3–6 into Eq. 2, and Eqs. 8–11 into Eq. 7, then the final expression due to conduction based on the surface-contact hollow cubic structure can be written as

$$
\begin{aligned}
k_c = \Bigg\{ & \frac{(2-\gamma_b)\gamma_a^2\gamma_b}{1-(1-\alpha)\gamma_a} + \frac{\gamma_a^2[(1-\gamma_b)^2-\gamma_c^2]}{1-(1-\alpha)\gamma_a\gamma_b} + \frac{2\gamma_a\gamma_c(1-\gamma_a)}{1-(1-\alpha)\gamma_a\gamma_c} \\
& + \frac{\gamma_a^2\gamma_c^2}{\alpha+(1-\alpha)(1-\gamma_b)\gamma_a} + (1-\gamma_a)(1+\gamma_a-2\gamma_a\gamma_c) \Bigg\} k_g, \qquad \text{when } 0 < c < a-2h \\
k_c = \Bigg\{ & \frac{(1-\gamma_c^2)\gamma_a^2}{1-(1-\alpha)\gamma_a} + \frac{2\gamma_a\gamma_c(1-\gamma_a)}{1-(1-\alpha)\gamma_a\gamma_c} + \frac{\gamma_a^2[\gamma_c^2-(1-\gamma_b)^2]}{\alpha} \\
& + \frac{(1-\gamma_b)^2\gamma_a^2}{\gamma_a(1-\gamma_b)+(1-\gamma_a+\gamma_a\gamma_b)\alpha} + 1 \qquad \text{when } a > c > a-2h \\
& + \gamma_a(1-\gamma_a-2\gamma_c+\gamma_a\gamma_c) \Bigg\} k_g,
\end{aligned}
\tag{12}
$$

where $\alpha = k_g/k_{cq}$. Apparently, this effective conductivity expression is dependent on the thermal conductivity of the shell, the thermal conductivity of the gas, and microstructures of the xonotlite as well as the porosity of the shell.

2.2 Radiative Heat Transfer

In practical applications, the optical thickness of an insulation material is typically very large. The optical thickness (τ) is defined as the product of the extinction coefficient and the thickness of the insulation material. For an optically thick medium ($\tau \gg 1$), radiation travels only a short distance before being scattered or absorbed. The local intensity is the result of radiation from only nearby positions being considered. For this situation it is possible to transform the integral relation for the radiative energy into a diffusion relation like that for heat conduction. It is called the diffusion approximation, and the radiative heat flux can be expressed as [15]

$$
q_r = -\frac{4}{3\rho K_{e,m}}\frac{\partial e_b}{\partial x} = -\frac{16}{3\rho K_{e,m}}\sigma T^3\frac{\partial T}{\partial x} \tag{13}
$$

Hence, the total effective thermal conductivity due to both conduction and radiation is defined as

$$
k_e = k_c + k_r = k_c + \frac{16\sigma}{3\rho K_{e,m}}T^3 \tag{14}
$$

where T is the medium local temperature, e_b is the blackbody emissive power, σ is the Stefan–Boltzmann constant, k_r is the radiative thermal conductivity, ρ is the medium density, and $K_{e,m}$ is the specific Rossland mean extinction coefficient, and calculated as

$$
\frac{1}{K_{e,m}} = \int_0^\infty \frac{1}{K_{\lambda,m}}\frac{\partial e_{b\lambda}}{\partial T}\mathrm{d}\lambda \Big/ \int_0^\infty \frac{\partial e_{b\lambda}}{\partial T}\mathrm{d}\lambda = \int_0^\infty \frac{1}{K_{\lambda,m}}\frac{\partial e_{b\lambda}}{\partial e_b}\mathrm{d}\lambda \tag{15}
$$

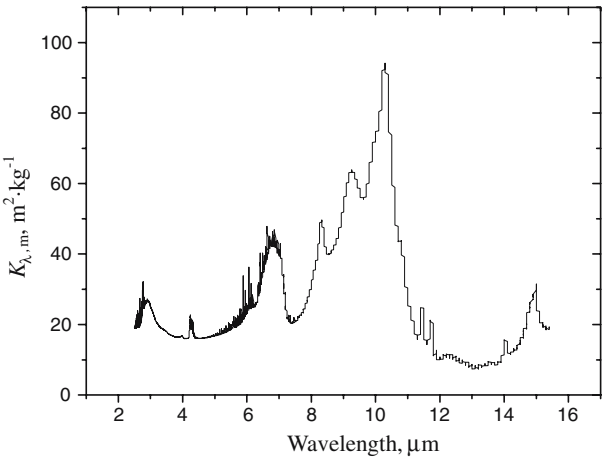

Fig. 3 Spectral specific extinction coefficient of xonotlite

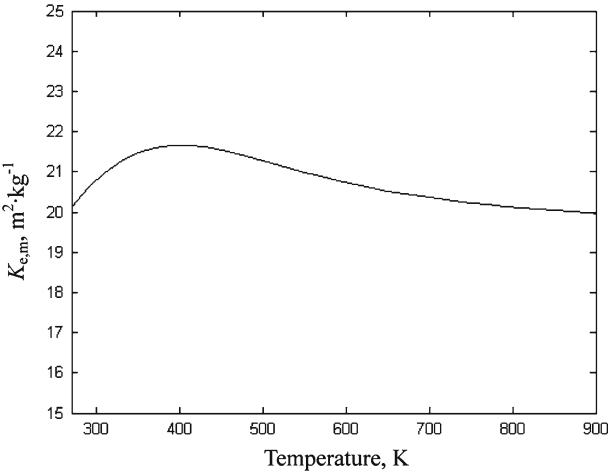

Fig. 4 Specific Rossland mean extinction coefficient of xonotlite

where $e_{b\lambda}$ is the spectral blackbody emissive power and $K_{\lambda,m}$ is the spectral specific extinction coefficient. For a homogeneous material, $K_{\lambda,m}$ is the inherent parameter and independent of the density of the medium. The specific Rossland mean extinction coefficient is an average value of $K_{\lambda,m}$ weighted by the local spectral energy flux. If $K_{\lambda,m}$ is measured, we can obtain $K_{e,m}$ from Eq. 15, and calculate the radiative conductivity from Eq. 14.

3 Experimental

3.1 Infrared Spectral Measurements

For intermediate temperature (200–700 K) applications, most thermal energy radiates in the spectral range between 2 and 16 μm approximately. The spectral specific extinction coefficients usually can be derived from transmission measurements on a thin insulation sample performed with a Fourier transform infrared (FTIR) spectrometer. The xonotlite-type calcium silicate samples are measured [16] with a Nicolet Spectrum NEXUS670 model of FTIR with a spectrum range from 400 to 4000 cm^{-1}. The results (Fig. 3) show that the specific extinction coefficients are larger than 7 $\mathrm{m}^2 \cdot \mathrm{kg}^{-1}$ over the whole measured spectral range, and the maximum value is about 94 $\mathrm{m}^2 \cdot \mathrm{kg}^{-1}$. Figure 4 depicts the variation of the specific Rossland mean extinction coefficient $K_{e,m}$ with temperature for the measured sample. Since $K_{e,m}$ is an average extinction coefficient over the spectrum weighted by the emissive power, it represents the ability to extinguish thermal radiation at a certain temperature. It is shown that $K_{e,m}$ increases at first and then decreases slightly with an increase in temperature. A maximum of $K_{e,m}$ exists at about 400 K. According to Wien's displacement law, when the temperature is 400 K, the corresponding wavelength at which the spectral emissive power is maximum is 7.2 μm. Figure 2 shows that the specific spectral extinction coefficient of xonotlite has a peak value at about 7 μm, and this accounts for the maximum of $K_{e,m}$ at 400 K. Another peak value of $K_{\lambda,m}$ also exists at about 10 μm; the corresponding temperature at which the spectral emissive power is a maximum is 289.8 K. $K_{e,m}$ does not increase due to the fact that the peak value of $K_{\lambda,m}$ has little influence on radiative properties of the medium for the spectral emissive power curve is flat at low temperature according to Planck's law.

3.2 Thermal Conductivity Measurements

The transient hot-strip method was used to measure the thermal conductivity of xonotlite insulation material of different densities. The principle of this technique is reported by Gustafsson et al. [17]. An electric current is passed through the hot strip pressed between two slabs of the sample of equal size, and the temperature of the strip increases. The rate at which the temperature of the strip increases depends on the thermal conductivity of the sample. This is the basis for thermal-conductivity measurements with the transient hot-strip method. The result for the thermal conductivity is calculated as $k = P_0/(4\pi)/[\mathrm{d}T(t)/\mathrm{d}\ln(t)]$, where P_0 is the power input to the strip, t is the time, and $\mathrm{d}T(t)/\mathrm{d}\ln(t)$ is the slope of temperature versus $\ln(t)$ after several seconds of heating. In order to measure the thermal conductivity of xonotlite at different temperatures and pressures, two conditions are satisfied for the transient hot-strip method used in this work. A vacuum chamber permits measurements of the thermal conductivity from 0.01 Pa to atmospheric pressure at ambient temperature; an electric furnace permits measurements of the thermal conductivity of xonotlite from ambient temperature to as high as 970 K. A 2.0 mm (width) $\times$ 0.1 mm (thickness) nickel–chrome (Ni80Cr20) strip is used as the heating source. The temperatures are measured using Type K 0.1 mm

Table 1 Temperature dependence of measured thermal conductivity of xonotlite at atmospheric pressure

$124.5\,\mathrm{kg\cdot m^{-3}}$		$165\,\mathrm{kg\cdot m^{-3}}$		$199.4\,\mathrm{kg\cdot m^{-3}}$		$234\,\mathrm{kg\cdot m^{-3}}$	
T (K)	k ($\mathrm{W\cdot m^{-1}\cdot K^{-1}}$)	T(K)	k ($\mathrm{W\cdot m^{-1}\cdot K^{-1}}$)	T(K)	k ($\mathrm{W\cdot m^{-1}\cdot K^{-1}}$)	T (K)	k ($\mathrm{W\cdot m^{-1}\cdot K^{-1}}$)
296	0.0416	294	0.0468	293	0.0574	295	0.0639
433	0.0528	421	0.0545	433	0.0617	430	0.0676
526	0.0694	533	0.0682	557	0.0699	552	0.0778
678	0.0937	643	0.0848	679	0.0789	671	0.0874
821	0.141	773	0.111	823	0.1002	811	0.1015
947	0.199	978	0.199	935	0.142		

Table 2 Pressure dependence of measured thermal conductivity in $\mathrm{W\cdot m^{-1}\cdot K^{-1}}$ of xonotlite at ambient temperature

p (Pa)	$124.5\,\mathrm{kg\cdot m^{-3}}$	$165\,\mathrm{kg\cdot m^{-3}}$	$199.4\,\mathrm{kg\cdot m^{-3}}$	$234\,\mathrm{kg\cdot m^{-3}}$
0.045	0.00881	0.0165	0.0282	0.0296
5	0.00889	0.0162	0.0284	0.0293
50	0.00971	0.0163	0.0282	0.0295
110	0.011	0.0176	0.0281	0.0308
300	0.0132	0.0185	0.0297	0.0329
800	0.0212	0.0243	0.0327	0.0355
5000	0.0326	0.0356	0.0409	0.0425
30000	0.0385	0.0433	0.0498	0.0533
101325	0.0416	0.0468	0.0574	0.0639

diameter thermocouples welded on the strip surface. Four samples with different densities are measured as shown in Tables 1 and 2. The reproducibility is better than 3% at ambient temperature, and better than 6% at 773 K.

4 Calculations

For calculations with the conductive heat transfer model, some additional information is needed.

4.1 Effective Thermal Conductivity of the Shell k_{cq}

The shell of xonotlite secondary particles is formed by interwoven xonotlite fiber. Some pores also exist in it. Here, we adopt the parallel model to estimate the effective thermal conductivity of the shell: $k_{cq} = (1 - \Phi_i)k_s + \Phi_i k_g$, where k_s is the thermal conductivity of xonotlite fiber.

4.2 Gaseous Thermal Conductivity in High-Porosity Xonotlite k_g

The gaseous thermal conductivity increases with pressure as an 'S' shape depending upon the degree of collisions between gas molecules and gas/wall interactions. A

Table 3 Date for estimation of the thermal conductivity in $W \cdot m^{-1} \cdot K^{-1}$ of xonotlite fiber

T (K)	300	400	500	600	700	800	900	1000
k_{SiO_2}	1.3792	1.5058	1.6265	1.7625	1.9349	2.1649	2.4736	2.8822
k_{CaO}	1.2511	1.2329	1.2122	1.1890	1.1632	1.1349	1.1041	1.0707
k_{H_2O}	0.6094	0.6828	0.6575	0.6223	0.6658	0.8767	1.3436	2.1552

frequently used formula [18,19] for the calculation of the gaseous thermal conductivity in porous media is expressed as

$$k_g = k_g^0(T)/(1 + 2\zeta Kn) \tag{16}$$

where ζ is a constant specific to the gas in the pores (for air $\zeta \approx 2$) and $k_g^0(T)$ is the temperature-dependent gaseous thermal conductivity at atmospheric pressure. The thermal conductivity value for air from the literature [20] is adopted for $k_g^0(T)$. Kn is the Knudsen number defined as

$$Kn = l_m/d_m \tag{17}$$

where d_m is a characteristic system size, which is the mean pore size of xonotlite in this study. It is shown (Fig. 6) that the model matches well with experimental results when d_m=20 μm. The result coincides with the measured value for d_m in the literature [3,4]. l_m is the mean free path of gas molecules in free space, calculated as

$$l_m = \frac{1}{\sqrt{2} n_g \pi d_g^2} = \frac{k_B T}{\sqrt{2}\pi d_g^2 p} \tag{18}$$

where n_g is the number density of gas molecules, k_B is the Boltzmann constant ($k_B = 1.38 \times 10^{-23}\,J \cdot K^{-1}$), T and p are the gas temperature and pressure, and d_g is the diameter of a gas molecule ($d_g = 3.798 \times 10^{-10}$ m for nitrogen).

4.3 Solid Thermal Conductivity of Xonotlite Fiber k_s

There are no available data of the thermal conductivity of pure xonotlite fiber. An estimation of the thermal conductivity of fiber in xonotlite is $k_s = (f_1 k_{SiO_2} + f_2 k_{CaO} + f_3 k_{H_2O})$ according to the molecular formula of xonotlite $6CaO \cdot 6SiO_2 \cdot H_2O$, where f_1, f_2, and f_3 are the mole fractions of silicon dioxide, calcium oxide, and water, respectively, and k_{SiO_2}, k_{CaO}, and k_{H_2O} are the thermal conductivities of silicon dioxide, calcium oxide, and water, respectively. The thermal conductivity data in Table 3 are used to estimate k_s according to the data given in the literature [21].

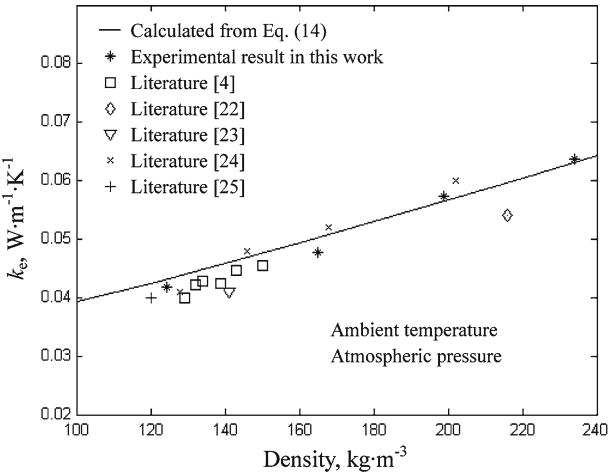

Fig. 5 Density dependence of thermal conductivity of xonotlite insulation material and comparisons with literature data

5 Comparisons with Experimental Data

Figures 5–7 show comparisons of the experimental data from this work and the literature [4,22–25] with the theoretical model. In the calculations, $h = 4\,\mu$m and $a - 2h = d_m = 20\,\mu$m are adopted according to measured structural values of xonotlite in the literature [3,4]. It is shown that the theoretical model matches well with experimental data when $\gamma_a = 0.19$, $\phi_i = 0.3$, and γ_c is calculated from Eq. 1. Figure 6 and Table 2 show that the thermal conductivity of xonotlite decreases significantly with a drop of pressure and reaches a minimum value at about 100 Pa. The thermal conductivity of xonotlite is mainly attributed to solid conduction and radiation. It indicates that the gaseous thermal conductivity is the main part in the total conductivity of xonotlite, and the solid thermal conductivity is not large. It is shown that the thermal conductivity of xonotlite with $\rho = 124.5\,\mathrm{kg}\cdot\mathrm{m}^{-3}$ due to solid conduction and radiation is only $0.0089\,\mathrm{W}\cdot\mathrm{m}^{-1}\cdot\mathrm{K}^{-1}$ at ambient temperature.

It is shown (Fig. 7) that the thermal conductivity of xonotlite increases significantly with an increase in temperature. The agreement between the theoretical model and experimental data also indicates that the spectral specific extinction coefficients derived from the transmittance measurements on a thin insulation sample performed with a Fourier transform infrared (FTIR) spectrometer are accurate, and can be used to calculate the radiative properties in xonotlite insulation material.

6 Summary

The effective thermal conductivity of high-porosity xonotlite insulation material has been investigated experimentally as a function of pressure and temperature. Specific extinction coefficient spectra have been obtained by measuring the transmittance spectrum of xonotlite samples of different thicknesses with a FTIR spectrometer. A

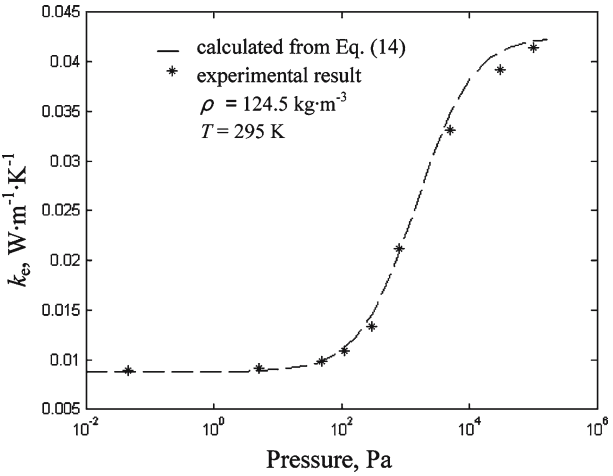

Fig. 6 Pressure dependence of thermal conductivity of xonotlite insulation material

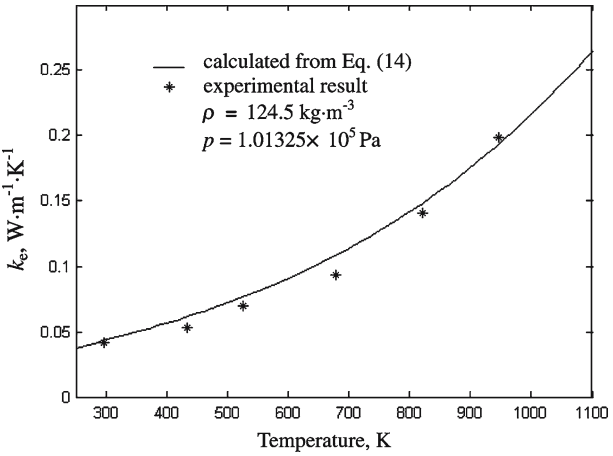

Fig. 7 Temperature dependence of thermal conductivity of xonotlite

theoretical model for conductive thermal conductivity has also been developed based on the surface-contact hollow cubic structure. It is shown that the model matches extremely well with the experimental data. It is expected that the validated effective thermal conductivity model will be important for the thermal design and thermal analysis of xonotlite insulation material.

Acknowledgment This research was financially supported by the National Natural Science Foundation of China (No. 50276003).

References

1. N.W. Wieslawa, Cement Concrete Res. **29**, 1759 (1999)
2. W. Ni, Z.Y. Cao, X.L. Shu, China Petrol. Mach. **24**, 495 [in Chinese] (1996)
3. M.Q. Li, F.Y. Chen, S.Q. Xia, J.H. Li, H.X. Liang, J. Chinese Ceram. Soc. **28**, 401 [in Chinese] (2000)
4. Q.J. Zheng, W. Wang, Brit. Ceram. Trans **99**, 187 (2000)
5. L.W. Hrubesh, R.W. Pekala, J. Mater. Res. **9**, 731 (1994)
6. P.J. Burns, C.L. Tien, Int. J. Heat Mass Transfer **22**, 929 (1979)
7. H.W. Russell, J. Am. Ceram. Soc. **18**, 1 (1935)
8. D. Kunii, J.M. Smith, AICHE J. **6**, 71 (1960)
9. P. Zehner, E.U. Schlunder, Chem. Ing. Tech. **42**, 933 (1970)
10. S. Nozad, R.G. Carbonell, S. Whitaker, Chem. Eng. Sci. **40**, 843 (1985)
11. L.S. Verma, A.K. Shrotriya, R. Singh, D.R. Chaudhary, J. Phys. D: Appl. Phys. **24**, 1729 (1991)
12. C.T. Hsu, P. Cheng, K.W. Wong, J. Heat Transfer **177**, 264 (1995)
13. F. Yu, G.S. Wei, X.X. Zhang, K. Chen, Int. J. Thermophys. **27**, 293 (2006)
14. K. Chen, F. Yu, X.X. Zhang, G.S. Wei, J. Univ. Sci. Technol. Beijing **26**, 650 (2004)
15. R. Siegel, J.R. Howell, *Thermal Radiation Heat Transfer* (Taylor & Francis, London, 2002)
16. X.X. Zhang, G.S. Wei, F. Yu, J. Therm. Sci. **14**, 281 (2005)
17. S.E. Gustafsson, E. Karawack, M.N. Khan, J. Phys. D: Appl. Phys. **12**, 1411 (1979)
18. X. Lu, M.C. Ardunini-Schuster, J. Kuhn, O. Nilsson, J. Fricke, R.W. Pekala, Science **221**, 971 (1992)
19. O.J. Lee, K.H. Lee, T.J. Yim, S.Y. Kim, K.P. Yoo, J. Non-Cryst. Solids **298**, 287 (2002)
20. Y.S. Touloukian, P.E. Liley, S.C. Saxena, *Thermal Conductivity: Nonmetallic Liquids and Gases* (IFI/Plenum, New York, 1970)
21. Y.S. Touloukian, P.E. Liley, S.C. Saxena, *Thermal Conductivity: Nonmetallic Solids* (IFI/Plenum, New York, 1970)
22. W. Ni, Z.Y. Cao, X.L. Shu, J. Univ. Sci. Technol. Beijing **18**, 495 [in Chinese] (1996)
23. Z.J. Mao, J.X. Sheng, Bull. Chinese Ceram. Soc. **1**, 50 [in Chinese] (1997)
24. C.L. Fang, D.S. Song, Non-Metallic Mines. **23**, 28 [in Chinese] (2000)
25. Z.Y. Wang, Y.M. Huang, M.M. Wu, G.Q. Xue, Naihuo Cailiao. **31**, 134 [in Chinese] (1997)